

Accepted Manuscript

Influence of YbP on the thermoelectric properties of *n*-type P doped Sig₅Ge₅ alloy

Fan Sui, Sabah K. Bux, Susan M. Kauzlarich

PII: S0925-8388(18)30635-2

DOI: [10.1016/j.jallcom.2018.02.184](https://doi.org/10.1016/j.jallcom.2018.02.184)

Reference: JALCOM 45060

To appear in: *Journal of Alloys and Compounds*

Received Date: 13 November 2017

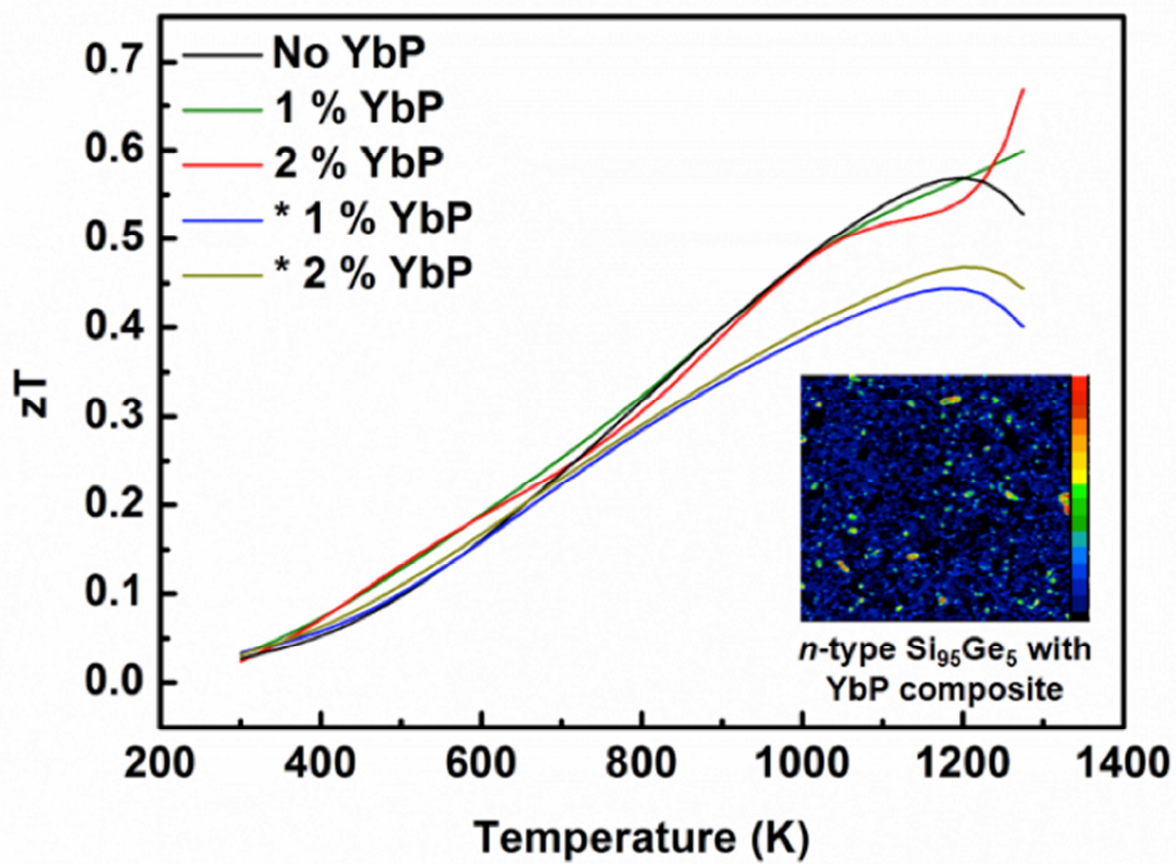
Revised Date: 13 February 2018

Accepted Date: 14 February 2018

Please cite this article as: F. Sui, S.K. Bux, S.M. Kauzlarich, Influence of YbP on the thermoelectric properties of *n*-type P doped Sig₅Ge₅ alloy, *Journal of Alloys and Compounds* (2018), doi: 10.1016/j.jallcom.2018.02.184.

This is a PDF file of an unedited manuscript that has been accepted for publication. As a service to our customers we are providing this early version of the manuscript. The manuscript will undergo copyediting, typesetting, and review of the resulting proof before it is published in its final form. Please note that during the production process errors may be discovered which could affect the content, and all legal disclaimers that apply to the journal pertain.





Influence of YbP on the thermoelectric properties of *n*-type P doped Si₉₅Ge₅ alloy

Fan Sui^{1,2}, Sabah K. Bux³ and Susan M. Kauzlarich^{1}*

¹Department of Chemistry, University of California, One Shields Avenue, Davis, California 95616

²Center for Information Photonics and Energy Materials, Shenzhen Institutes of Advanced Technology, Chinese Academy of Sciences, 518055, China

³Thermal Energy Conversion Technologies and Advancement Group, Jet Propulsion Laboratory, California Institute of Technology, 4800 Oak Grove Drive, MS 277-207, Pasadena

*Email: smkauzlarich@ucdavis.edu

Keywords: Thermoelectric materials; mechanochemical processing; thermoelectric transport; Silicon

Abstract:

Since the report of high *zT* in Si₉₅Ge₅ there has been significant interest in low Ge alloy compositions for thermoelectric applications. The application of YbP was explored as a means to lower thermal conductivity. A series of 3 % phosphorus (P) doped *n*-type Si₉₅Ge₅ (SiGe) alloy was reacted with YbH₂ (0, 1, 2%). YbP was formed in the SiGe alloy matrix from the reaction between YbH₂ and P during the Spark Plasma Sintering (SPS) process. Thermoelectric property measurements were performed on sintered pellets from room temperature to 1273 K. X-ray diffraction patterns were collected from the ground powder samples and confirmed the main phase possessed diamond structured Si₉₅Ge₅ (space group: *Fd $\bar{3}m$*) as well as the presence of YbP (space group: *Fm $\bar{3}m$*). The carrier concentration of the sample was controlled by the amount of YbH₂ added, removing some of the phosphorus to form YbP. *n*-type Si₉₅Ge₅ alloy samples with higher YbP amounts showed higher electrical resistivity and lower thermal conductivity attributed to loss of the P dopant. Another composite series of *n*-type Si₉₅Ge₅ with YbP were synthesized with additional P compositions (1, 2 %). The thermoelectric properties were characterized from room temperature to 1273 K, and the samples possess electrical resistivity, carrier concentrations, and thermal conductivity as expected from the additional P dopant. The presence of YbP lowered lattice thermal conductivity when the sample was appropriately doped. The Seebeck coefficients were measured with both off-axis and uniaxial axis experimental configurations. These results show that the off-axis measurements overestimate the Seebeck coefficients of the Si₉₅Ge₅ alloy samples. This is attributed to a cold finger effect and therefore only the uniaxial data are combined for *zT* calculations. The *n*-type Si₉₅Ge₅ samples with YbP and less than 3 % P dopant show similar *zT* compared with the Si₉₅Ge₅ sample with no YbP inclusions and 3 % P dopant with a peak *zT* of 0.6 at 1200 K.

1. Introduction:

Large amounts of heat are generated as a by-product from the energy consumption of gasoline, coal and natural gas combustion. Thermoelectric materials, defined by the Seebeck Effect, can enhance the energy efficiency ratio by the direct conversion of electricity from waste heat.¹ The challenge for thermoelectric devices to achieve wide applications is to convert waste heat into electricity efficiently. Thermoelectric efficiency is related by the figure of merit zT , which is defined by $\alpha^2 T / \rho \kappa$. zT will be maximized along with the thermoelectric conversion efficiency for materials with a high Seebeck coefficient (α , $\mu\text{V}/\text{K}$), low electrical resistivity (ρ , $\text{m}\Omega\cdot\text{cm}$) and low thermal conductivity (κ , $\text{mW}/\text{cm}\cdot\text{K}$); however, these parameters are interrelated and to decouple them is challenging.²

There are a variety of energy consumption processes that generate high temperature waste heat above 1000 K, for example, power plants and vehicle engines. Thermoelectric materials for high temperature applications need to be thermally stable in the high temperature range and also provide good thermoelectric performance at the corresponding operating temperature. So far, SiGe alloys are one of the most studied thermoelectric materials for high temperatures.^{2, 3} $\text{Si}_{80}\text{Ge}_{20}$ alloys have been applied in Radioisotope Thermoelectric Generators (RTGs) which generate electricity for space system from the heat released by the nuclear decay of radioactive isotopes.³

n -type bulk SiGe alloys achieved a peak zT of about 1.0 in the temperature range of 900 ~ 950 °C in the 1990s.⁴ Properly doped SiGe alloys have high powder factors ($\alpha^2\sigma$) but also high thermal conductivity of around 5 W/m·K. Thermoelectric properties of SiGe alloys can be greatly enhanced if the thermal conductivity can be further reduced. High energy ball milling processes have been employed to prepare nanostructured and doped SiGe alloys. The nano-size grain boundaries were shown to decrease lattice thermal conductivity to below 1 W/m·K and enhance the zT of n -type $\text{Si}_{80}\text{Ge}_{20}$ alloy to 1.84 at 1073 K characterized by off-axis Seebeck measurement.^{5, 6} While the reported thermal conductivity decrease is convincing, the zT value is suspicious because the work failed to correct the off-axis Seebeck measurement error introduced by the cold-finger effect, which will be discussed in this work. This method also successfully enhanced the zT of boron doped p -type $\text{Si}_{95}\text{Ge}_5$ to 0.95 at 900 °C, 90 % higher than the currently used RTG thermoelectric leg.⁷ $\text{Si}_{95}\text{Ge}_5$ with low Ge content, has also been studied.^{8, 9} Low Ge content makes SiGe alloys more likely for wide-spread industrial applications, as Si is much more earth abundant than Ge.⁸ However, the lattice thermal conductivity of $\text{Si}_{95}\text{Ge}_5$ alloy is higher than $\text{Si}_{80}\text{Ge}_{20}$ alloy because there is less alloy scattering from Ge substitution. Nanostructured n -type $\text{Si}_{95}\text{Ge}_5$ alloy synthesized from high energy ball mill route was studied and

showed increased short range phonon scattering and therefore achieved a comparable zT of 0.95 to the $\text{Si}_{80}\text{Ge}_{20}$ used in RTG but with significantly less Ge.⁸

Mingo *et al.* proposed an “Nanoparticle-in-Alloy” strategy to enhance zT 's in semiconductors; the basic idea is that nanoparticles embedded in an alloy matrix can lead to a lattice thermal conductivity reduction and thereby enhanced zT .¹⁰ Calculations showed the coexistence of scattering by individual atoms and nanoparticles can effectively decrease phonon mean free path and lead to a potential 5-fold increase in zT .¹⁰ One experimental example of this idea is seen in Yb-substituted Mg_2Si which showed lower thermal conductivity than plain Mg_2Si .¹¹ Yb was alloyed into the crystal structure of Mg_2Si to form $\text{Mg}_{2-x}\text{Yb}_x\text{Si}$ and excess Yb introduced Yb_3Si_5 inclusions in Mg_2Si matrix.¹¹ Therefore, the samples showed combined scattering effect at both low and high phonon frequencies from individual atoms and embedded clusters. Among the 0.2, 0.5, 1 % Yb substituted samples, 1 % Yb sample showed lowest thermal conductivity.¹¹ Besides silicide nanoparticles, other properly chosen nanoparticles embedded in a SiGe matrix have been studied as well. Modulation-doping has also been reported to increase thermoelectric power factor.^{12, 13} It was proposed that the good band alignment of the $\text{Si}_{70}\text{Ge}_{30}\text{P}_3$ nanoparticle and the SiGe matrix can promote the flow of charge carriers from nanoparticle to SiGe matrix and increase mobility as well as electrical conductivity.¹³ It was proposed that modulation doping of $\text{Si}_{70}\text{Ge}_{30}\text{P}_3$ could increase carrier mobility and decrease the lattice thermal conductivity of $\text{Si}_{95}\text{Ge}_5$ matrix. Overall, $\text{Si}_{70}\text{Ge}_{30}\text{P}_3$ in SiGe matrix lead to a zT of 1.3 ± 0.1 at 900 °C.¹³ This provides incentive for further research, as these data were obtained with the off-axis Seebeck measurement and should be validated.

n-type $\text{Si}_{95}\text{Ge}_5$ alloys multi-doped with GaP and P were reported to possess enhanced electrical conductivity and lower thermal conductivity than alloys doped with P only.⁹ We present our work of synthesizing *n*-type $\text{Si}_{95}\text{Ge}_5$ alloys with YbP introduced by the decomposition and chemical reaction of YbH_2 with P as well as the thermoelectric properties from room temperature to 1273 K. The ball milled metal hydride precursor allows for homogeneous distribution of the Yb element in the SiGe alloy matrix.¹⁴ Metal hydrides decompose and generate hydrogen which can be vented during either annealing or sintering processes in SPS (Spark Plasma Sintering), and provides a clean and convenient synthesis method.¹⁵ The thermoelectric properties of $\text{Si}_{95}\text{Ge}_5$ with YbP composite were characterized to examine the influence of YbP on the alloys' transport properties.

2. Experiments:

2.1 Synthesis:

Samples were synthesized by arc-melting of Si lump (Alfa Aesar, 99.99999+ %) and Ge pieces (Alfa Aesar, 99.999 %) with the molar ratio of 95 : 5 in an argon filled arc melting apparatus, where a pellet of pure Zr is initially melted to get rid of any oxygen before the sample being arc-melted. The arc-melted ingot was then ball milled

with 3 at % phosphorus (Johnson Matthey Chemicals, 99.9999%) with a SPEX SamplePrep 8000M Mixer/Mill for 16 hours (15 min on/off mode to prevent over heat) inside a 55 mL steel-jacketed tungsten carbide vial with tungsten carbide inserts. Two 8 mm and one 15 mm tungsten carbide balls were used for the ball milling process and the ball mill container was sealed in air-tight plastic bag filled with Ar to prevent any oxidation. A typical sample size was about 6 g in total. YbH₂ powder of 0, 1, 2 at % respectively, was added to the *n*-type Si₉₅Ge₅ alloy and ball milled for 30 min inside a 5 mL polymer ball mill container, sealed in an air-tight plastic bag. The YbH₂ powder was purchased as Yb powder (American Elements, 5N) and determined to be phase pure YbH₂ from powder X-ray diffraction. The sample sizes were ~ 1 gram each and the four samples were synthesized from the same batch of *n*-type Si₉₅Ge₅ (3 at % P), shown in Figure 1.

Another series of samples were synthesized in order to compensate for the loss of P from the SiGe matrix from the formation of YbP. Equal amounts of P and YbH₂ (1, 2 at %) were added to the *n*-type Si₉₅Ge₅ alloy (3 at % P, prepared as described above) in the ball mill container in order to investigate the addition of YbP with an excess amount of P dopant. In principle, these samples should result in 3% P dopant with additional YbP. These samples are labeled with * to distinguish from the first series of samples.

2.2 Spark Plasma Sintering (SPS):

Ball milled powders were sieved with 200 mesh filter inside an Ar filled glove box to prevent oxidation and loaded into a 12.7 mm diameter graphite die with graphite foil wrapped around the inner surface in glove box. The graphite foil prevents the pellets from cracking when removing them from the die after sintering. Samples were sintered using a Dr Sinter Lab Jr. at 950 °C for 15 mins and 47.4 MPa. All the pellets were fully sintered and greater than 98 % dense.

2.3 X-ray Diffraction (XRD):

Sintered pellets were polished with 400 grit SiC paper to remove graphite foil residues from the surface and ground into powder. X-ray diffraction patterns were collected on the ground powder samples utilizing a Bruker D8 diffractometer with Cu K α radiation ($\lambda = 1.5418 \text{ \AA}$). XRD patterns were also collected from ground powder samples of the pellets after thermoelectric property characterizations.

2.4 Electron Microprobe Analysis:

Fragments of the SPSed pellets were polished for microprobe analysis utilizing a Cameca SX-100 electron microprobe. The elemental composition and YbP inclusions were verified by X-ray elemental mapping of a typical 200 μm x 200 μm area with an electron accelerating voltage of 15 keV.

2.5 Thermoelectric property characterization:

Temperature dependent Hall coefficient and resistivity were measured with Van der Pauw 4-point tungsten probe measurement from room temperature to 1273 K at 0.8 T magnetic field. Samples were rapidly annealed in air to 1050 °C and then quenched to freeze the high solubility of P dopant in the matrix.¹⁶ Pressure was applied on the tungsten probes to assure good contact with the sample. The Seebeck coefficient of sintered 12.7 mm SiGe pellets was measured from 275 K to 1200 K with tungsten–niobium thermocouples under high vacuum in a custom apparatus.¹⁷ Thermal diffusivity was measured utilizing Netzsch LFA 404 system on the graphite coated pellets, which sat on SiC 12.7 mm sample holders.

Approximately 12 mm x 1.5 mm x 1.5 mm bars were cut from the center of the pellet with diamond saw. The sample bars were polished and their electrical resistivity and Seebeck coefficient were measured with a LSR-3 Linseis Seebeck and Electrical Resistivity Unit in the temperature range of 323 K to 1073 K. This measurement is a four probe off-axis measurement, *e.g.* the sample is clamped between upper and lower Pt electrodes and a pair of Pt thermocouples with a distance of 8 mm (total distance with the mid-distance being half the length of the bar) are placed off-axis.

3. Results and discussions:

3.1 Synthesis and sintering:

The X-ray diffraction (XRD) pattern collected from the 3 at % P doped Si₉₅Ge₅ powder after 16 hours ball milling is presented in Figure 1. All the peaks can be indexed with Si diamond structure ($Fd\bar{3}m$). XRD peaks are significantly broadened. Based on the pattern's peak FWHM, sample particle size is calculated to be 141 nm according to Williamson-Hall plot method, indicating the presence of nanocrystallites from 16 hours' ball milling process. After sintering the pellets were polished and their density was measured in toluene according to the Archimedes principle and listed in Table 1.

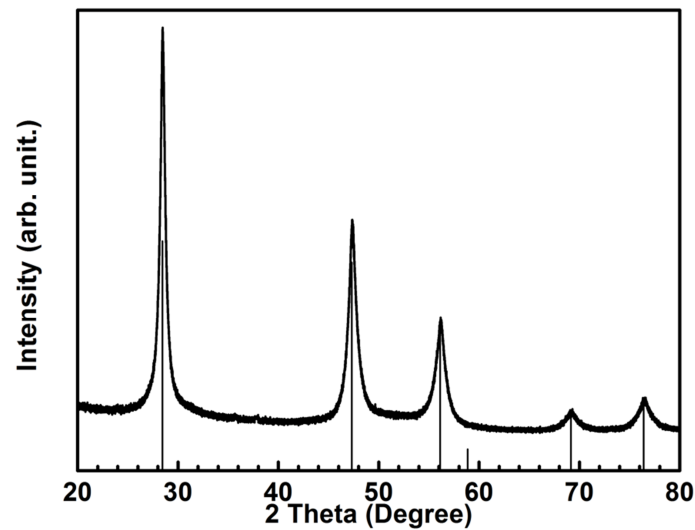


Figure 1. Powder XRD pattern of *n*-type $\text{Si}_{95}\text{Ge}_5$ (with 3 at % P) powder after 16 hours ball milling, used as starting material for all samples.

Table 1. Measured density (g/cm^3) of sintered $\text{Si}_{95}\text{Ge}_5$ pellets¹ at room temperature.

3 at % P doped $\text{Si}_{95}\text{Ge}_5$	No YbH_2	1 % YbH_2	2 % YbH_2	* 1 % YbH_2	* 2 % YbH_2
Sample I.D.	No YbP	1 % YbP	2 % YbP	* 1 % YbP	* 2 % YbP
Measured Density (g/cm^3)	2.48 (1)	2.56 (1)	2.62 (1)	2.59 (1)	2.67 (1)
Theoretical Density (g/cm^3)	2.50	2.55	2.60	2.55	2.60

¹All samples were prepared with 3 at % P dopant (Figure 1). The samples indicated with * had additional P added in an equivalent at % as the YbH_2 .

The powder XRD patterns are collected from the polished pellets of the first series of $\text{Si}_{95}\text{Ge}_5$ samples and results are shown in Figure 2. The samples with additional P added give similar XRD patterns. After the samples are sintered, the peak broadening is not seen in the XRD pattern, indicating that the grain size is significantly larger. Besides the $\text{Si}_{95}\text{Ge}_5$ main phase, the XRD pattern from YbP phase are present, indexed with the drop line in Figure 2. No YbSi_2 or any other Yb-Si phases are apparent in the sintered pellets. Yb reacts with the phosphorus dopant instead of SiGe alloy matrix during the SPS process, presumably due to the high mobility of P and the large formation energy of the rock salt structure. The relative diffraction intensity of

YbP increases with increasing amount of YbH₂. Therefore, Table 1 provides the YbH₂ starting percentages with their sample identification (I.D.) according to the following compositions: Si₉₅Ge₅ with 3 at % P (No YbP) 1 at % YbP and 2 at % P (1 % YbP), 2 at % YbP and 1 at % P (2 % YbP), 1 at % YbP and 3 at % P (*1 % YbP) and 2 at % YbP and 3 at % P (*2 % YbP).

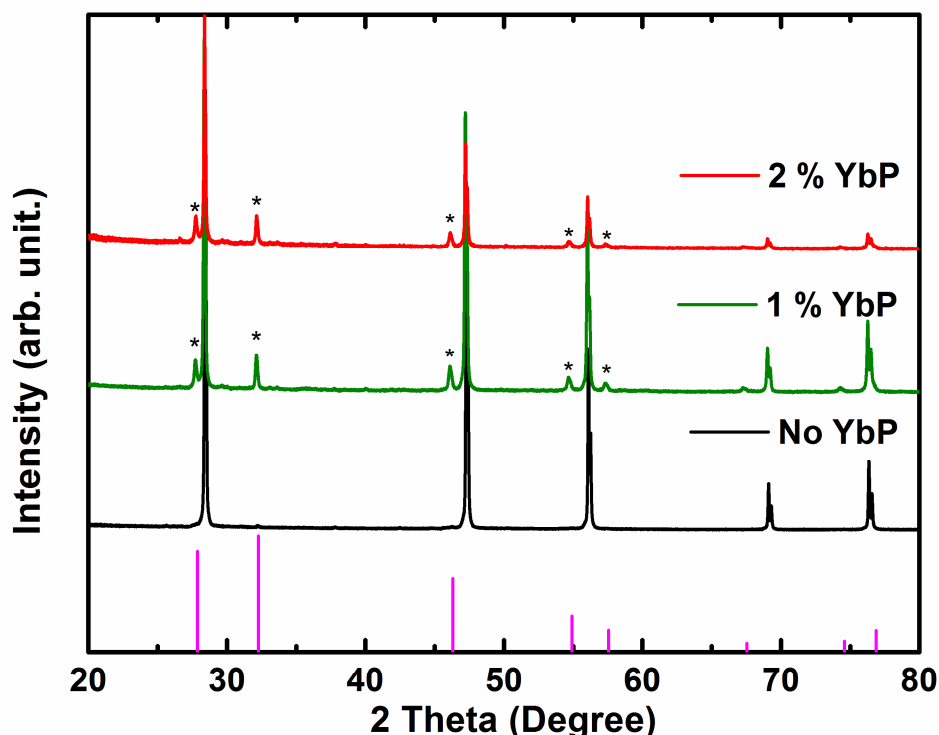


Figure 2. XRD pattern of sintered *n*-type Si₉₅Ge₅ pellets with the calculated pattern for the YbP phase indicated by the drop lines (PDF#47-1624). The diffraction peaks for YbP are indicated with *.

3.2 Electron microprobe analysis:

To understand the YbP phase distribution, electron microprobe analysis was performed on the polished sample surface. Yb element mapping images are shown in Figure 3. YbP particles are characterized by the Yb signal and are uniformly distributed throughout the samples.

Sample composition	1 % YbP	2 % YbP
--------------------	---------	---------

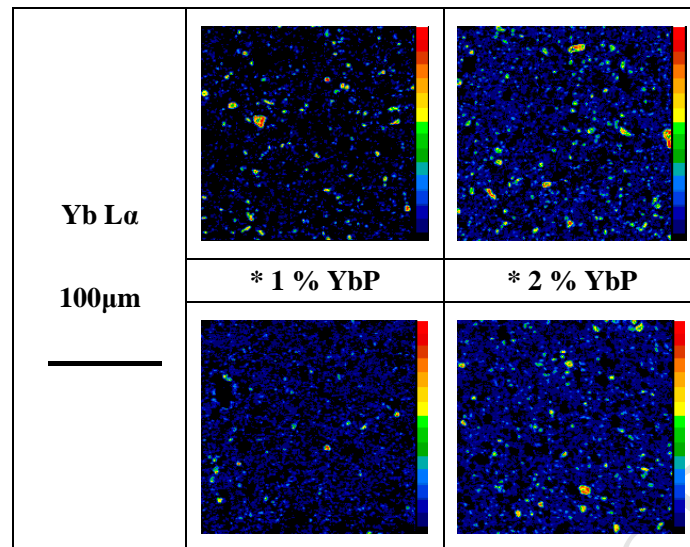


Figure 3. Yb elemental mapping of the $\text{Si}_{95}\text{Ge}_5$ samples with YbP and P doping with 15 keV electron accelerating voltage. The color corresponds to the relative elemental composition level according to the color bar shown at the right.

3.3 Transport properties:

Electrical resistivity of the *n*-type $\text{Si}_{95}\text{Ge}_5$ samples were measured from 275 K to 1273 K and plotted in Figure 4. The electrical resistivity of sintered $\text{Si}_{95}\text{Ge}_5$ samples show a similar trend in general as the electrical resistivity increases with increasing temperature and bends over when temperatures exceed 1000 K. In the samples of YbP with lesser amounts of P (1 % YbP and 2 % YbP), YbH_2 reacted with electron donor P during sintering process and as a result, samples with higher amounts of YbP possess higher electrical resistivity, which is not beneficial for thermoelectric conversion efficiency. 2 % YbP sample has a sharp transition, which may be attributed to YbP pinning the grain boundary at high temperature. In the case of the samples indicated with * (*1 % YbP, *2 % YbP), the YbH_2 content was equivalent to the additional P amount of 1 % and 2 %, thereby leaving the P dopant amount at 3 %. These samples show lower electrical resistivity, as expected. Unlike the multi-doped SiGe alloy with GaP and P,⁹ the presence of YbP does not reduce the electrical resistivity significantly and it is the P content that determines the measured resistivity. The electrical resistivity of the * samples also increases with temperature below 750 K but show an unusual sharp increase in the temperature range of 750 ~ 800 K and fluctuating in the temperature range of 800 ~ 1100 K. These temperature effects are also seen in the plain $\text{Si}_{95}\text{Ge}_5$ sample doped with 3 % P, but not the samples with less than 3 % P (1 % and 2 % YbP labeled samples). The fluctuation in electrical resistivity is attributed to P dopant precipitation kinetics at high temperature.¹⁸ Electrical resistivity decreases at temperatures exceeding 1100 K.

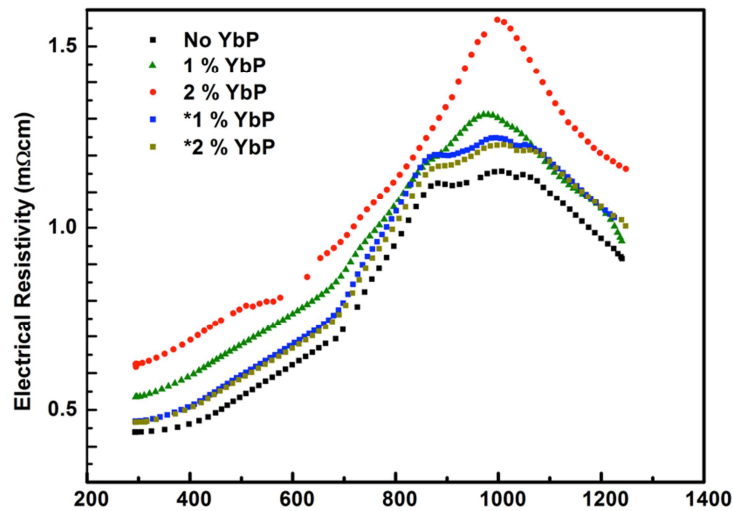


Figure 4. Electrical resistivity of *n*-type $\text{Si}_{95}\text{Ge}_5$ samples measured from 275 K to 1273 K. Electrical resistivity of $\text{Si}_{95}\text{Ge}_5$ samples are labeled according to YbP and P content with 3 at % P (No YbP), 1 at % YbP and 2 at % P (1 % YbP), 2 at % YbP and 1 at % P (2 % YbP), 1 at % YbP and 3 at % P (*1 % YbP) and 2 at % YbP and 3 at % P (*2 % YbP).

Hall measurements were performed on the $\text{Si}_{95}\text{Ge}_5$ samples to determine their carrier concentrations as well as mobility from 275 K to 1273 K (Figure 5). The values of the carrier concentration confirmed that the samples are heavily doped *n*-type semiconductors with electron carrier concentration in the range of $2 - 5 \times 10^{20} \text{ cm}^{-3}$ at room temperature. The sample with no YbP ($\text{Si}_{95}\text{Ge}_5$ with 3 % P) has an electron carrier concentration of about $5 \times 10^{20} \text{ cm}^{-3}$ from room temperature to about 700 K, above that temperature the carrier concentration decreases slightly and then increases above 900 K. The sample with 1 % YbP (with 2 % P) has a carrier concentration of $4 \times 10^{20} \text{ cm}^{-3}$. The sample with 2 % YbP (1 % P) is below $3 \times 10^{20} \text{ cm}^{-3}$. These results are consistent with the amount of P dopant. The samples with YbP and 3 % P (*1 % YbP and *2 % YbP) show carrier concentration of $4.5 \times 10^{20} \sim 5 \times 10^{20} \text{ cm}^{-3}$, similar to the 3 % P doped $\text{Si}_{95}\text{Ge}_5$ (No YbP) sample. The samples' mobility are in the same range, about $30 \text{ cm}^2/\text{Vs}$ at room temperature, and all the samples possess linearly decreasing mobility with increasing temperature.

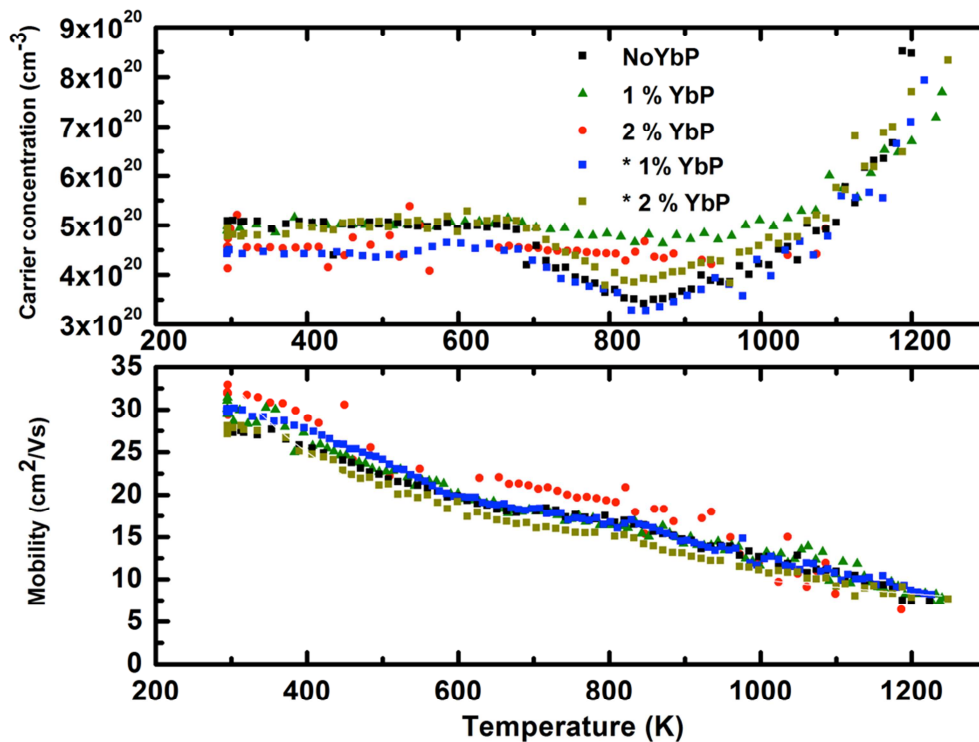


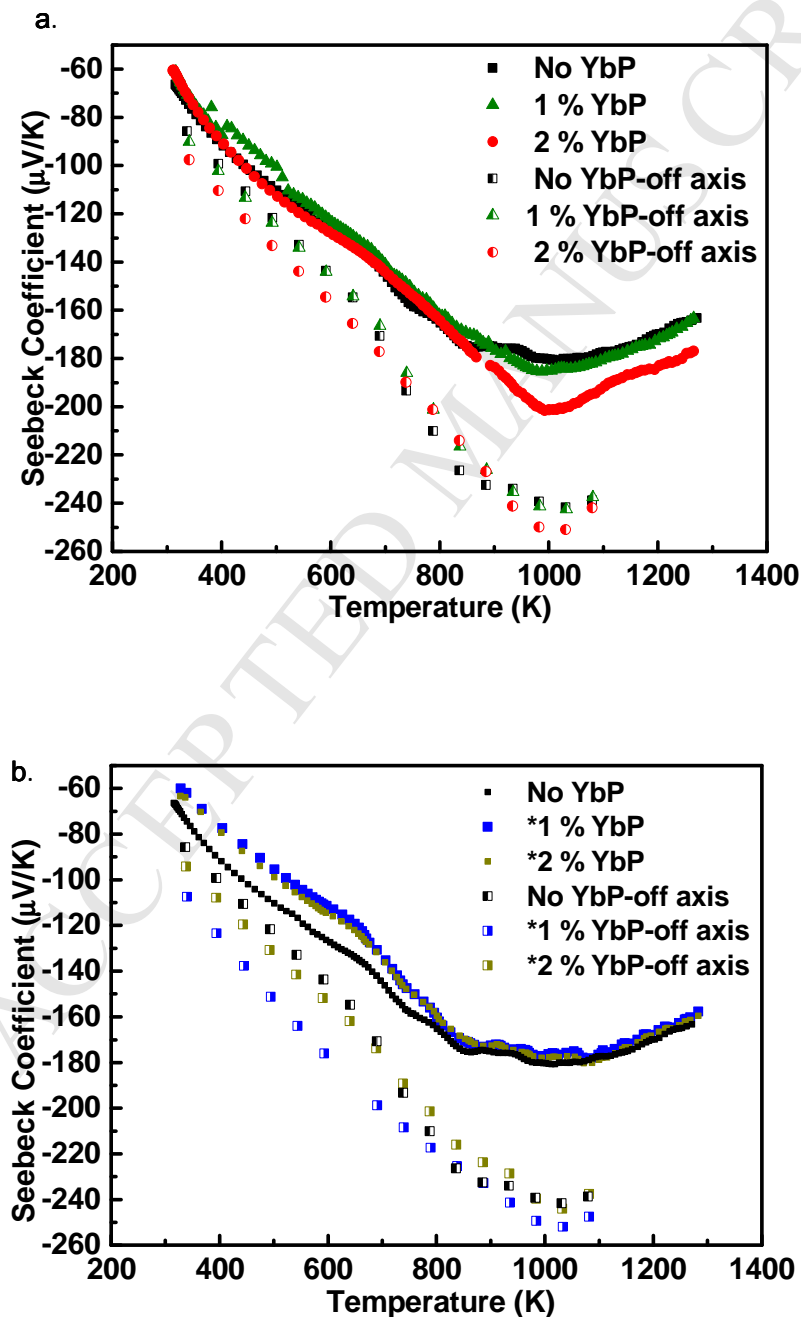
Figure 5. Charge carrier concentrations and mobility from Hall measurements in the temperature range of 275 K to 1275 K. $\text{Si}_{95}\text{Ge}_5$ samples are labeled according to YbP and P content with 3 at % P (No YbP), 1 at % YbP and 2 at % P (1 % YbP), 2 at % YbP and 1 at % P (2 % YbP), 1 at % YbP and 3 at % P (*1 % YbP) and 2 at % YbP and 3 at % P (*2 % YbP).

3.4 Seebeck coefficient measurement:

Sintered samples were measured twice with a custom uniaxial set up and a commercial four probe off-axis set up. In the uniaxial set up, absolute Seebeck coefficient was measured from 275 K to 1200 K under vacuum.

Figure 6 shows the Seebeck coefficient for the two series of samples with both experimental set-ups with the off-axis data indicated. Samples showed large negative Seebeck coefficients from about $-60 \mu\text{V/K}$ at 275 K and their absolute Seebeck coefficients increased with temperature until around 1000 K above which the values decreased which is attributed to the dopant precipitation kinetics. The Seebeck coefficients of the two series of samples are shown in the upper and lower figures separately. The $\text{Si}_{95}\text{Ge}_5$ sample with 2 % YbP content (1 % P dopant) from the first series of samples showed a maximum absolute Seebeck coefficient value of over $|-200| \mu\text{V/K}$ at about 1000 K, while no YbP (3 % P dopant) and 1 % YbP content (2 % P dopant) samples' Seebeck coefficient are in similar range and stay below

$|-200| \mu\text{V/K}$. In the second series of samples with the same amount of P dopant (3 %), the samples with 1 % and 2 % YbP content possess similar Seebeck coefficients. The Seebeck coefficient measurements showed that the off-axis measurement gave overestimated Seebeck coefficient of up to 25 % higher at 1000 K compared with the uniaxially measured Seebeck coefficient. This over-estimation has been described in the literature.¹⁸ One of the main differences between the two measurements is the position of thermocouples which measure temperature and voltage simultaneously. The Seebeck coefficient is obtained from $\Delta V/\Delta T$, therefore, the accurate reading of temperature from thermocouples is critical for Seebeck coefficient measurements.¹⁷



c.

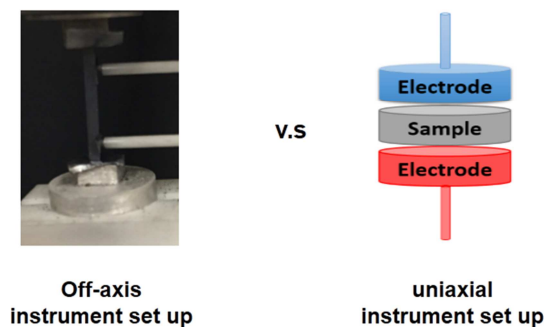


Figure 6. Comparisons of Seebeck coefficients measurements results from off-axis instrument set up and uniaxial set up on samples with no YbP and x % YbP ($x = 1, 2$) (a) with changing P dopant amounts and (b) 3 % P dopant. $\text{Si}_{95}\text{Ge}_5$ samples are labeled according to YbP and P content with 3 at % P (No YbP), 1 at % YbP and 2 at % P (1 % YbP), 2 at % YbP and 1 at % P (2 % YbP), 1 at % YbP and 3 at % P (*1 % YbP) and 2 at % YbP and 3 at % P (*2 % YbP); (c) Illustration of off axis and uniaxial instrument setup.

In the off-axis set up, the sample bars are clamped in between the Pt electrodes, and two Pt thermocouples are pressed against the sample off-axis. The measurement was performed under helium and graphite foils were used in between the sample and Pt electrodes to prevent a reaction at high temperature. The thermocouples can act as cold fingers (since they extend out of the furnace) at the contact position with the sample and underestimate the temperature gradient reading and therefore the Seebeck coefficients are overestimated.^{19, 20} In the uniaxial set up, the thermocouples are embedded through the heater and cold finger effect can be resolved, but as the thermocouples are in contact with the samples by constant pressure independently, the strength of the two thermocouples towards the sample can still affect the temperature reading.²⁰ This disagreement of Seebeck coefficient measurement results from different instrumental set up and increases with measurement temperature. Compare these two thermoelectric studies, $\text{Yb}_{14}\text{MnSb}_{11}$ with a large complex unit cell, possess thermal conductivity about ten times smaller than SiGe alloys.²¹ It is possible that the cold finger effect is more prominent on compounds with high thermal conductivity than the compounds with low thermal conductivity. As the off-axis set up of Seebeck coefficient measurements are common in commercial instruments (ZEM, Linseis, etc.), researchers should be aware of this temperature reading deviation in the Seebeck coefficient measurements of the SiGe alloys.^{19, 20}

3.5 Thermal transport properties:

The thermal conductivity of the $\text{Si}_{95}\text{Ge}_5$ samples were characterized from 275 K to 1275 K and plotted in Figure 7. The samples possess moderate thermal conductivity in the range of about 60 ~ 70 mW/cmK. This value of thermal conductivity is lower than what is reported for bulk $\text{Si}_{95}\text{Ge}_5$, but higher than $\text{Si}_{80}\text{Ge}_{20}$ alloys used in RTG

(below 50mW/cmK).^{6,9} Samples with YbP inclusions and less than 3 % P dopant (1% YbP and 2% YbP) show lower total thermal conductivity but the two * samples with 3% P possess higher thermal conductivity, likely contributed from the over doping and P at the grain boundaries.

To examine the influence of YbP composites on the lattice thermal conductivity, the electrical thermal conductivity were calculated with the Wiedemann-Franz equation, $\kappa = LT/\rho$, in which the measured electrical resistivity at the same temperature range was used and L was $2.22 \times 10^{-8} \text{ W } \Omega \text{ K}^{-2}$.²¹ The lattice thermal conductivity was shown in Figure 7, estimated by subtracting electrical thermal conductivity from the total thermal conductivity.

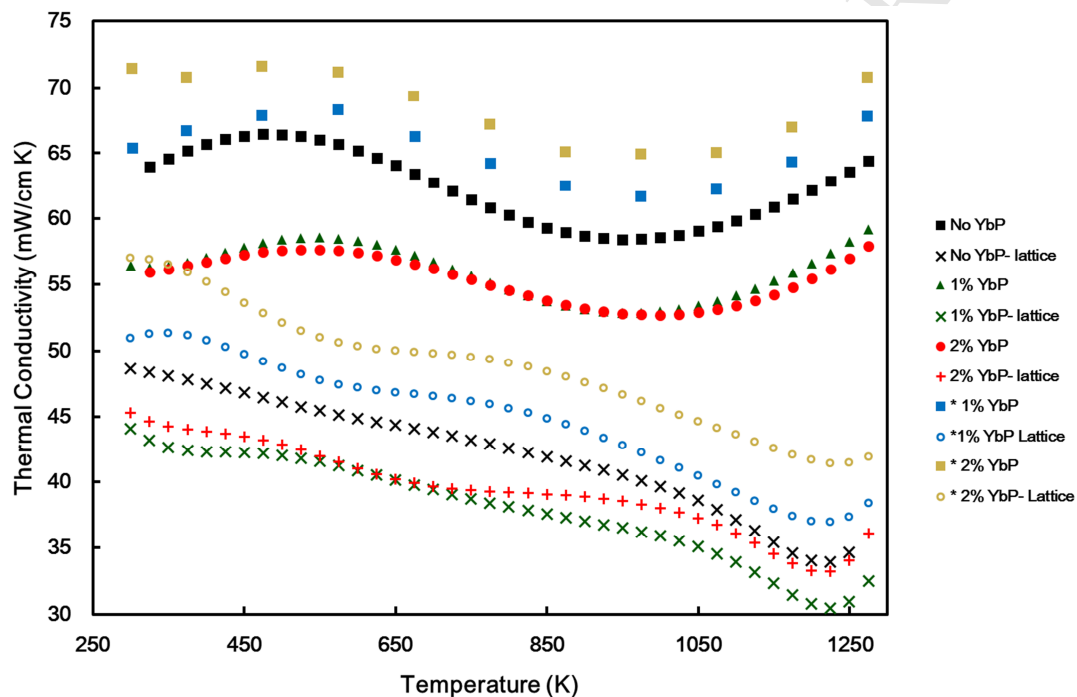


Figure 7. Thermal conductivity vs. temperature from laser flash measurements and calculated lattice thermal conductivity. $\text{Si}_{95}\text{Ge}_5$ samples are labeled according to YbP and P content with 3 at % P (No YbP), 1 at % YbP and 2 at % P (1 % YbP), 2 at % YbP and 1 at % P (2 % YbP), 1 at % YbP and 3 at % P (*1 % YbP) and 2 at % YbP and 3 at % P (*2 % YbP).

After estimating the electron and phonon contributions to the total thermal conductivity, the YbP composites with less than 3 % P were found to influence the thermal conductivity by decreasing the lattice thermal conductivity. The 3% P doped samples (indicated with *) with YbP showed higher lattice thermal conductivity than the no YbP phase reference sample (no YbP and 3 % P doping), which is likely to be attributed to the P precipitation behavior with higher P level at high temperature.¹⁶

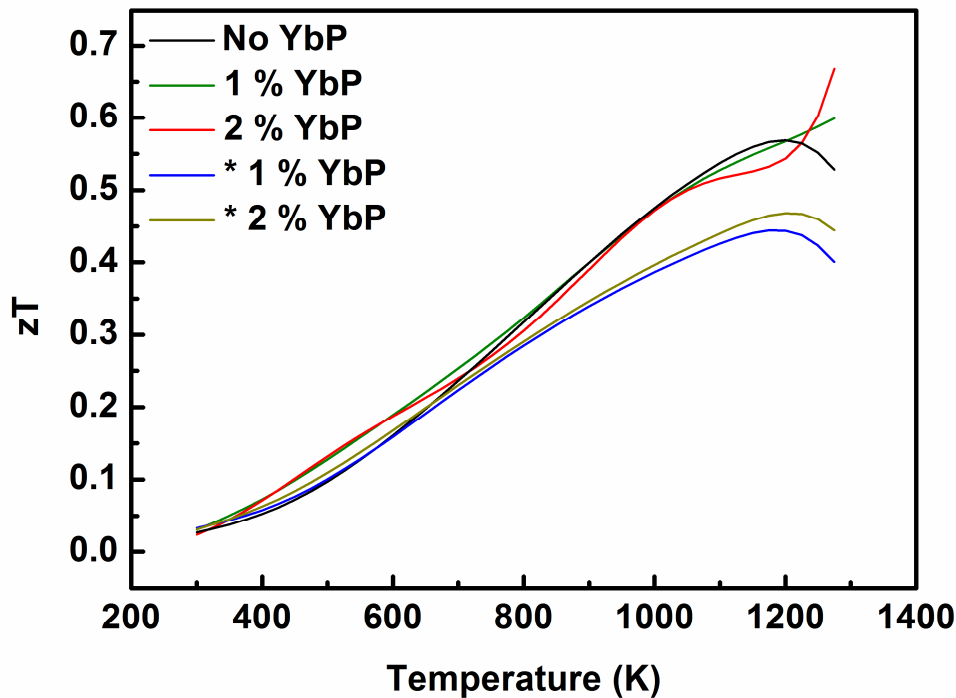


Figure 8. The figure of merit of *n*-type $\text{Si}_{95}\text{Ge}_5$ composite samples with YbP. $\text{Si}_{95}\text{Ge}_5$ samples are labeled according to YbP and P content with 3 at % P (No YbP), 1 at % YbP and 2 at % P (1 % YbP), 2 at % YbP and 1 at % P (2 % YbP), 1 at % YbP and 3 at % P (*1 % YbP) and 2 at % YbP and 3 at % P (*2 % YbP).

The figure of merit of *n*-type $\text{Si}_{95}\text{Ge}_5$ composite samples with YbP is provided in Figure 8 and were calculated from the polynomial fits of measured electrical resistivity, Seebeck coefficient (from the uniaxial instrumental set up) and thermal conductivity. As discussed above, more exciting data could be presented by applying off-axis Seebeck data, but this type of measurement provides high Seebeck values due to a cold-finger effect. The $\text{Si}_{95}\text{Ge}_5$ sample with 3 % P (No YbP), 1 % YbP with 2 % P (1% YbP) and 2 % YbP with 1 % P (2% YbP) show similar values of zT increasing with temperature. As the thermoelectric properties are interrelated by carrier concentration, the similarity of results of the YbP containing samples to the (No YbP) sample is attributed to the improved absolute Seebeck coefficient and lower thermal conductivity, mainly from decreased carrier concentration. Compared to *n*-type $\text{Si}_{80}\text{Ge}_{20}$ alloys which have a reported peak zT of 1 in the temperature range of 900 to 950 °C, the low Ge content of $\text{Si}_{95}\text{Ge}_5$ samples studied herein possess lower figures of merit. The YbP inclusions in the matrix provide a smaller effect than the amount of dopant on the experimental transport properties. The zT of the * samples containing both YbP and 3 % P bend over at temperatures exceeding 1200 K and show lower zT due to higher thermal conductivity.

4. Conclusion:

n-type Si₉₅Ge₅ alloy with 3% P dopant was synthesized through 16 hours of ball milling with P. YbP was introduced to the alloy matrix during SPS sintering process with YbH₂ as a starting material. The reaction of YbH₂ with P to form YbP tunes the carrier concentration of the composite of Si₉₅Ge₅ as YbH₂ reacts with the P, which is the electron donor. The sintered composite samples are dense pellets with the diameter of 12.7 mm. To understand the influence of YbP on the samples' thermoelectric properties, two series of samples were synthesized in the same manner: one with decreasing P content (P removed by addition of YbH₂ to form YbP), the second one with constant 3 % P (P added stoichiometrically with YbH₂ to compensate the amount of YbP formed in situ). The samples' thermoelectric properties were fully characterized. The deviation of up to 25 % between uniaxial and off-axis configured instruments that measure Seebeck coefficients are documented, consistent with a cold finger effect observed in off-axis measurements. Because of the combined effect of increased electrical resistivity and decreased lattice thermal conductivity, the YbP with less than 3 % P samples remain consistent with the modest *zT* observed in 3% P doped Si₉₅Ge₅. The efforts to compensate P loss by additional P amount during ball milling process failed to lead to *zT* enhancement, because the excess P dopant in the matrix leads to higher thermal conductivity.

5. Acknowledgements: The authors thank Gregory Baxter and Nick Botto for sample polishing and the electron microprobe measurements. Financial support from the DOE Office of Nuclear Energy's Nuclear Energy University Programs and NSF DMR-1405973 is gratefully acknowledged. Part of this research was carried out at the Jet Propulsion Laboratory, California Institute of Technology, under a contract with the National Aeronautics and Space Administration. This work was supported by the NASA Science Mission Directorate's Radioisotope Power Systems program.

6. Reference:

1. Slack, G. A., *CRC Handbook of Thermoelectrics*, edited by D. M. Rowe. CRC press: Boca Raton, FL, 1995.
2. Snyder, G. J.; Toberer, E. S., Complex thermoelectric materials. *Nature Materials* **2008**, 7 (2), 105-114.
3. Schmidt, G. R.; Dudzinski, L. A.; Sutliff, T. J., *Radioisotope power: A key technology for deep space exploration*. INTECH Open Access Publisher: 2011.
4. Koumoto, K.; Mori, T., *Thermoelectric Nanomaterials: Materials Design and Applications*. Springer Heidelberg, 2013; Vol. 182.
5. Basu, R.; Bhattacharya, S.; Bhatt, R.; Roy, M.; Ahmad, S.; Singh, A.; Navaneethan, M.; Hayakawa, Y.; Aswal, D. K.; Gupta, S. K., Improved thermoelectric performance of hot pressed nanostructured *n*-type SiGe bulk alloys. *J. Mater. Chem. A* **2014**, 2 (19), 6922-6930.
6. Wang, X. W.; Lee, H.; Lan, Y. C.; Zhu, G. H.; Joshi, G.; Wang, D. Z.; Yang, J.; Muto, A. J.; Tang, M. Y.; Klatsky, J.; Song, S.; Dresselhaus, M. S.; Chen, G.; Ren, Z.

- F., Enhanced thermoelectric figure of merit in nanostructured n-type silicon germanium bulk alloy. *Appl. Phys. Lett.* **2008**, *93* (19), 193121.
7. Joshi, G.; Lee, H.; Lan, Y.; Wang, X.; Zhu, G.; Wang, D.; Gould, R. W.; Cuff, D. C.; Tang, M. Y.; Dresselhaus, M. S.; Chen, G.; Ren, Z., Enhanced Thermoelectric Figure-of-Merit in Nanostructured p-type Silicon Germanium Bulk Alloys. *Nano Lett.* **2008**, *8* (12), 4670-4674.
8. Zhu, G. H.; Lee, H.; Lan, Y. C.; Wang, X. W.; Joshi, G.; Wang, D. Z.; Yang, J.; Vashaee, D.; Guilbert, H.; Pillitteri, A.; Dresselhaus, M. S.; Chen, G.; Ren, Z. F., Increased Phonon Scattering by Nanograins and Point Defects in Nanostructured Silicon with a Low Concentration of Germanium. *Phys. Rev. Lett.* **2009**, *102* (19), 196803.
9. Xu, Y.-d.; Xu, G.-y.; Ge, C.-c., Improvement in thermoelectric properties of n-type Si₉₅Ge₅ alloys by heavy multi-dopants. *Scripta Mater.* **2008**, *58* (12), 1070-1073.
10. Mingo, N.; Hauser, D.; Kobayashi, N. P.; Plissonnier, M.; Shakouri, A., "Nanoparticle-in-Alloy" Approach to Efficient Thermoelectrics: Silicides in SiGe. *Nano Lett.* **2009**, *9* (2), 711-715.
11. Janka, O.; Zaikina, J.; Bux, S.; Tabatabaifar, H.; Yang, H.; Browning, N. D.; Kauzlarich, S. M., Microstructure Investigations of Yb-substituted Mg₂Si for Thermoelectric Applications. In *J. Mater. Chem. C*, 2016.
12. Liao, B.; Chen, G., Nanocomposites for thermoelectrics and thermal engineering. *MRS Bull.* **2015**, *40* (9), 746-752.
13. Yu, B.; Zebajadi, M.; Wang, H.; Lukas, K.; Wang, H.; Wang, D.; Opeil, C.; Dresselhaus, M.; Chen, G.; Ren, Z., Enhancement of Thermoelectric Properties by Modulation-Doping in Silicon Germanium Alloy Nanocomposites. *Nano Lett.* **2012**, *12* (4), 2077-2082.
14. Zaikina, J. V.; Batuk, M.; Abakumov, A. M.; Navrotsky, A.; Kauzlarich, S. M., Facile Synthesis of Ba_{1-x}K_xFe₂As₂ Superconductors via Hydride Route. *J. Am. Chem. Soc.* **2014**, *136* (48), 16932-16939.
15. Sui, F.; He, H.; Bobev, S.; Zhao, J.; Osterloh, F. E.; Kauzlarich, S. M., Synthesis, Structure, Thermoelectric Properties, and Band Gaps of Alkali Metal Containing Type I Clathrates: A₈Ga₈Si₃₈ (A = K, Rb, Cs) and K₈Al₈Si₃₈. *Chem. Mater.* **2015**, *27* (8), 2812-2820.
16. Bux, S. K.; Blair, R. G.; Gogna, P. K.; Lee, H.; Chen, G.; Dresselhaus, M. S.; Kaner, R. B.; Fleurial, J.-P., Nanostructured Bulk Silicon as an Effective Thermoelectric Material. *Ad. Func. Mater.* **2009**, *19* (15), 2445-2452.
17. Wood, C.; Chmielewski, A.; Zoltan, D., Measurement of Seebeck coefficient using a large thermal gradient. *Rev. Sci. Instrum.* **1988**, *59* (6), 951-954.
18. Dunham, S. T., MODELING OF THE KINETICS OF DOPANT PRECIPITATION IN SILICON. *J. Electrochem. Soc.* **1995**, *142* (8), 2823-2828.
19. Joshua, M., Protocols for the high temperature measurement of the Seebeck coefficient in thermoelectric materials. *Meas. Sci. Technol.* **2013**, *24* (8), 085601.
20. Borup, K. A.; de Boor, J.; Wang, H.; Drymiotis, F.; Gascoin, F.; Shi, X.; Chen, L.; Fedorov, M. I.; Muller, E.; Iversen, B. B.; Snyder, G. J., Measuring thermoelectric

transport properties of materials. *Energy Environ. Sci.* **2015**, 8 (2), 423-435.

21. Grebenkemper, J. H.; Hu, Y. F.; Barrett, D.; Gogna, P.; Huang, C. K.; Bux, S. K.; Kaulzarich, S. M., High Temperature Thermoelectric Properties of Yb₁₄MnSb₁₁ Prepared from Reaction of MnSb with the Elements. *Chem. Mater.* **2015**, 27 (16), 5791-5798.

21. Kumar, G. S.; Prasad, G.; Pohl, R. O., Experimental determinations of the Lorenz number. *J. Mater. Sci.* 1993, 28 (16), 4261-4272.

ACCEPTED MANUSCRIPT

Highlights

- A new composite phase of YbP with phosphorus (P) doped $\text{Si}_{195}\text{Ge}_5$ (SiGe) alloy
- YbP lowers lattice thermal conductivity when the sample is appropriately doped
- Off-axis measurements overestimate the Seebeck coefficients of $\text{Si}_{195}\text{Ge}_5$ alloys

ACCEPTED MANUSCRIPT